Supporting Information

The Role of Nitrogen Sources and Hydrogen Adsorption on the Dynamic Stability of Fe-N-C Catalysts in Oxygen Reduction Reaction

Zhou Huang, Fuhua Li, Yongduo Liu, Siguo Chen, Zidong Wei, * *and Qing Tang**

[a]School of Chemistry and Chemical Engineering, Chongqing Key Laboratory of Theoretical and Computational Chemistry, Chongqing University, Chongqing 401331, China

*E-mail: zdwei@cqu.edu.cn; qingtang@cqu.edu.cn

Table of Contents

We constructed a Fe−N_4 doped-graphene/water interface (Fe−N−C), added 36 H_2O molecules with a density of 1 g cm^{-3} to the system and introduced an extra hydrogen atom which would decompose into a hydronium and an electron spontaneously to represent the counter charge within the EDL. We performed 5ps with 10000 steps of ab initio molecular dynamics (AIMD) simulation. The changes in energies and temperatures during the AIMD simulation are shown in Figure S1, indicating that the structure is well-equilibrated.

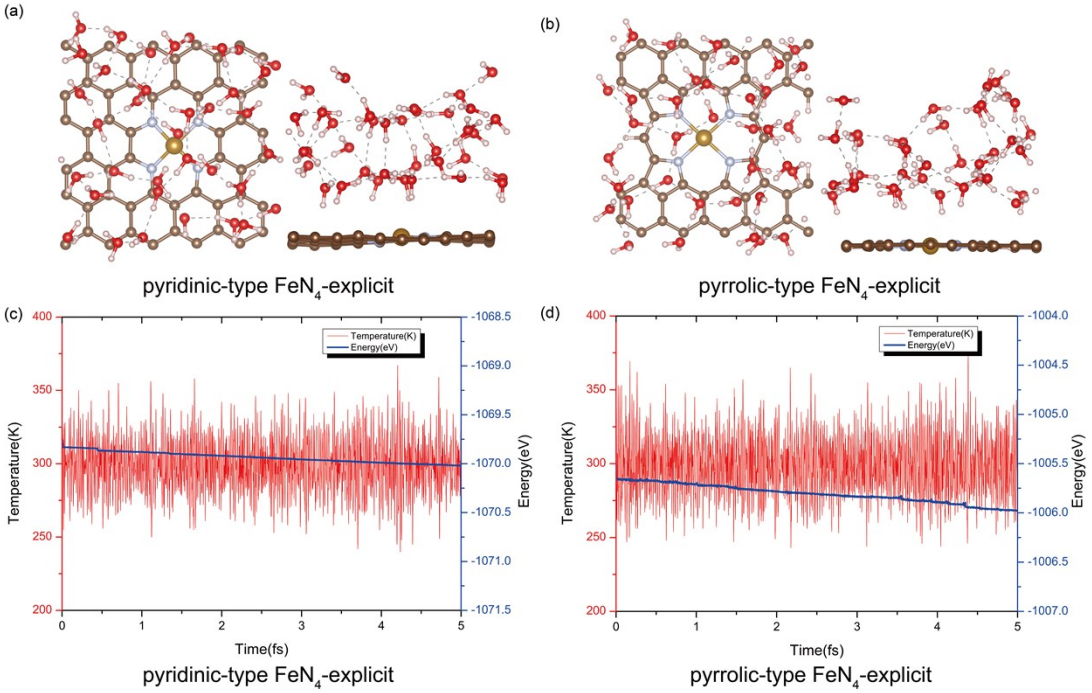

Figure S1. The snapshot structures of pyrrolic-type FeN_4-explicit (a) and pyrrolic-type FeN_4-explicit (b) after 5ps MD simulations; MD energy and temperature profiles for pyrrolic-type FeN_4-explicit (c) and pyrrolic-type FeN_4-explicit (d) during 5 ps AIMD simulations.

To evaluate the dynamic process of iron atom leaching from the surface, an inert helium atom is fixed directly above the Fe atom at a distance of 14.9 Å. Bader charge analysis indicated that the He atom maintains two electrons, which has a negligible effect on the charge of the whole system. Herein, the He atom is just equivalent to the role of a rivet.

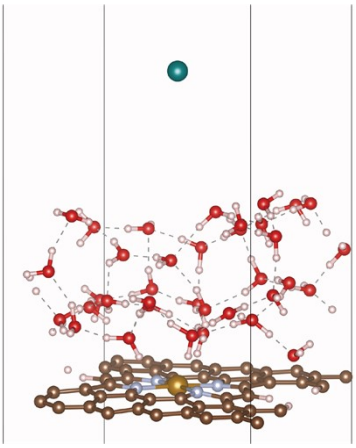

Figure S2. Full-size view of Fe−N_4 doped-graphene with 36 explicit water molecules used in our molecular dynamic simulations. Hydrogen bonds are represented by the dashed lines. C: gray; N: blue; Fe: brown; O: red; H: white; He: green.

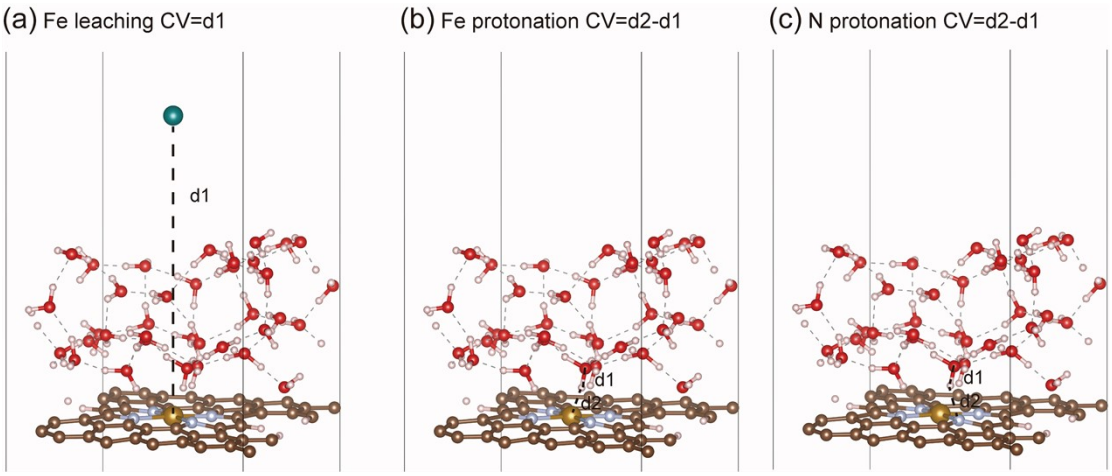

Figure S3. Illustrations of CV setting in the "slow-growth" method for the reaction of (a) Fe leaching, (b) hydrogen adsorption on Fe and (c) hydrogen adsorption on N.

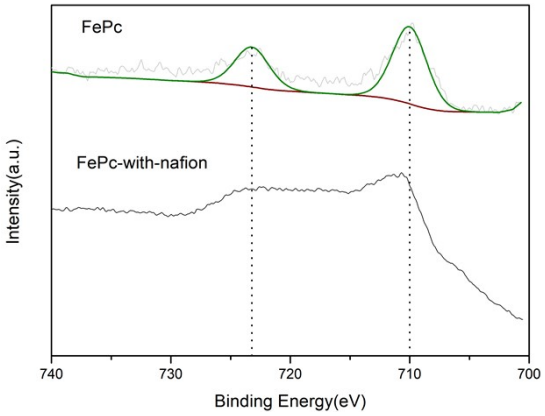

Figure S4. The Fe 2p XPS spectrum of the FePc molecule and the FePc molecule with nafion.

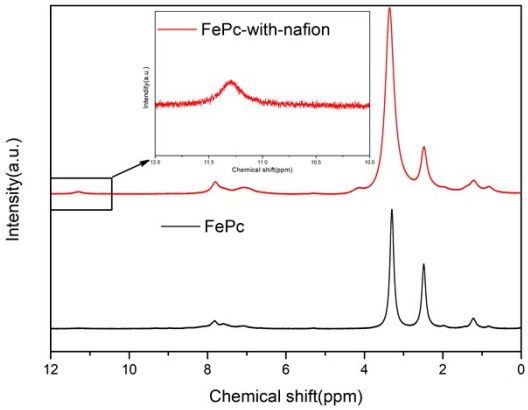

Figure S5. ^{1}H NMR spectra of FePc-with-Nafion and FePc in DMSO-d_6.

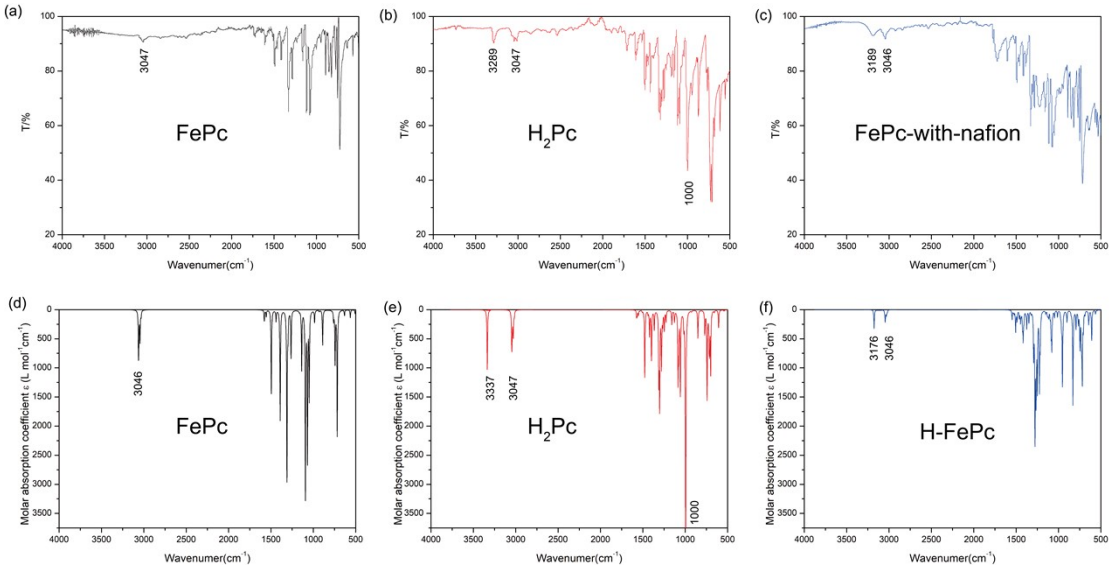

Figure S6. Experimental FT-IR spectra of FePc (a), H_2Pc (b) and FePc-with-Nafion (c); Simulated FT-IR spectra of FePc (d), H_2Pc (e) and H-FePc(f).

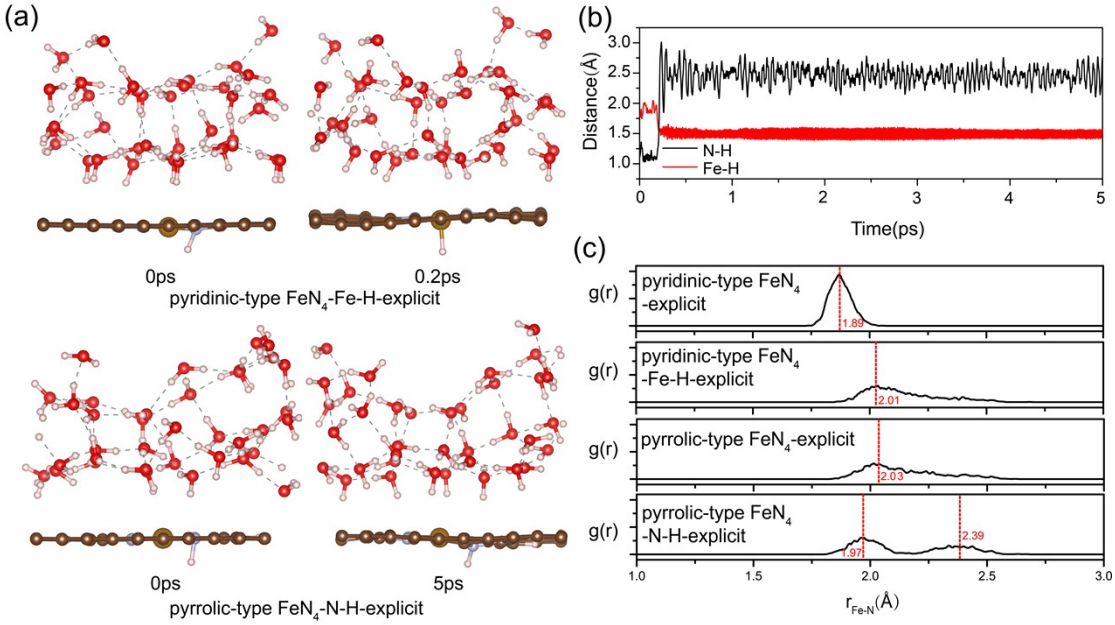

Figure S7. (a) AIMD simulation snapshots of nitrogen protonation in pyridinic-type FeN_4 and pyrrolic-type FeN_4 with explicit water. (b) An unconstrained 5 ps AIMD simulation representing the bond lengths of N-H and Fe-H in pyridinic-type FeN_4-N-H. (c) Radial Distribution Functions (RDFs) showcasing the Fe-N distance in bare and protonated pyridinic-type FeN_4 and pyrrolic-type FeN_4 with explicit water at 300 K, within a 5 ps time frame of the AIMD simulation.

Constant Potential Corrections

The simulations are done at constant charge [the number of electrons (*Ne*) is fixed], which means that the work functions (Φ) change along the reaction pathway. After the chemisorption of ORR intermediates, there will be some Φ variations, leading to the potential deviated from the targeted potential[1-5]. The energy difference caused Φ variations is:

$$\Delta E_{\Phi_1-\Phi_2} = E_{\Phi_1} - E_{\Phi_2} = \frac{\Delta q \times \Delta\Phi}{2} \quad (1)$$

The Δq and $\Delta\Phi$ are the interfacial charge and work function difference between the states of pristine and adsorbed one. Since the interfacial charge difference is hard to be accurately obtained, we can use the capacitance (C) defined in formula (3) to replace Δq:

$$C = \frac{\Delta q}{\Delta\Phi} \quad (2)$$

We then substitute the Δq in (3) with (4)

$$\Delta E_{\Phi_1-\Phi_2} = \frac{C \times \Delta\Phi^2}{2} \quad (3)$$

We calculate C from the change in the work function as the number of total electrons is varied. For the pyrrolic-type FeN_4 surface, the calculated C is 0.72 e/V. We found that the energy variations have little effect (< 0.1 eV). Therefore, we use one C value (0.72 e/V) in our calculation.

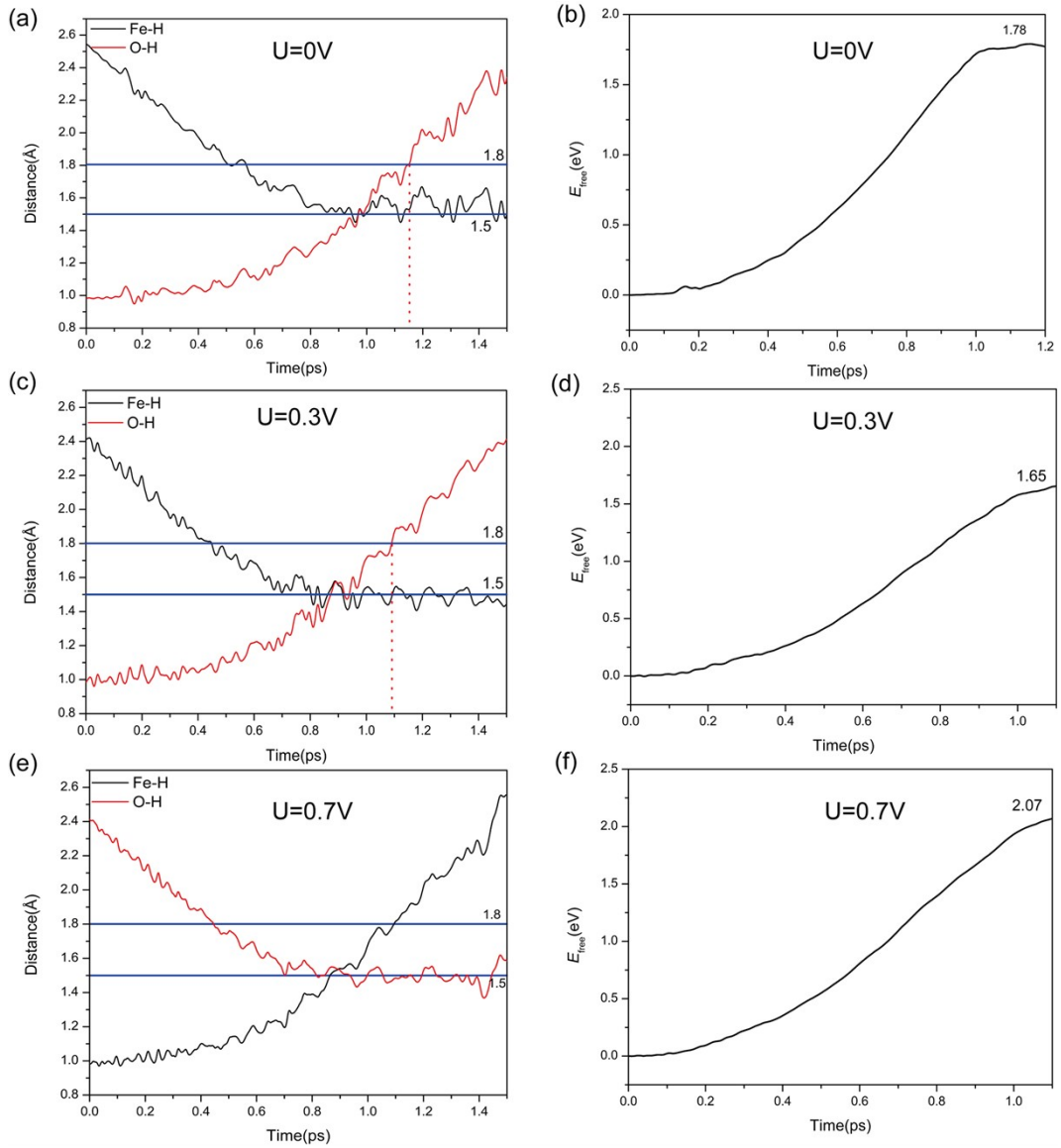

Figure S8. Dynamic evolution of bond lengths of Fe-H and O-H, as well as free energy profiles along the reaction coordinate in the pyrrolic-type FeN_4-explicit system, considering the iron protonation process under various potentials.

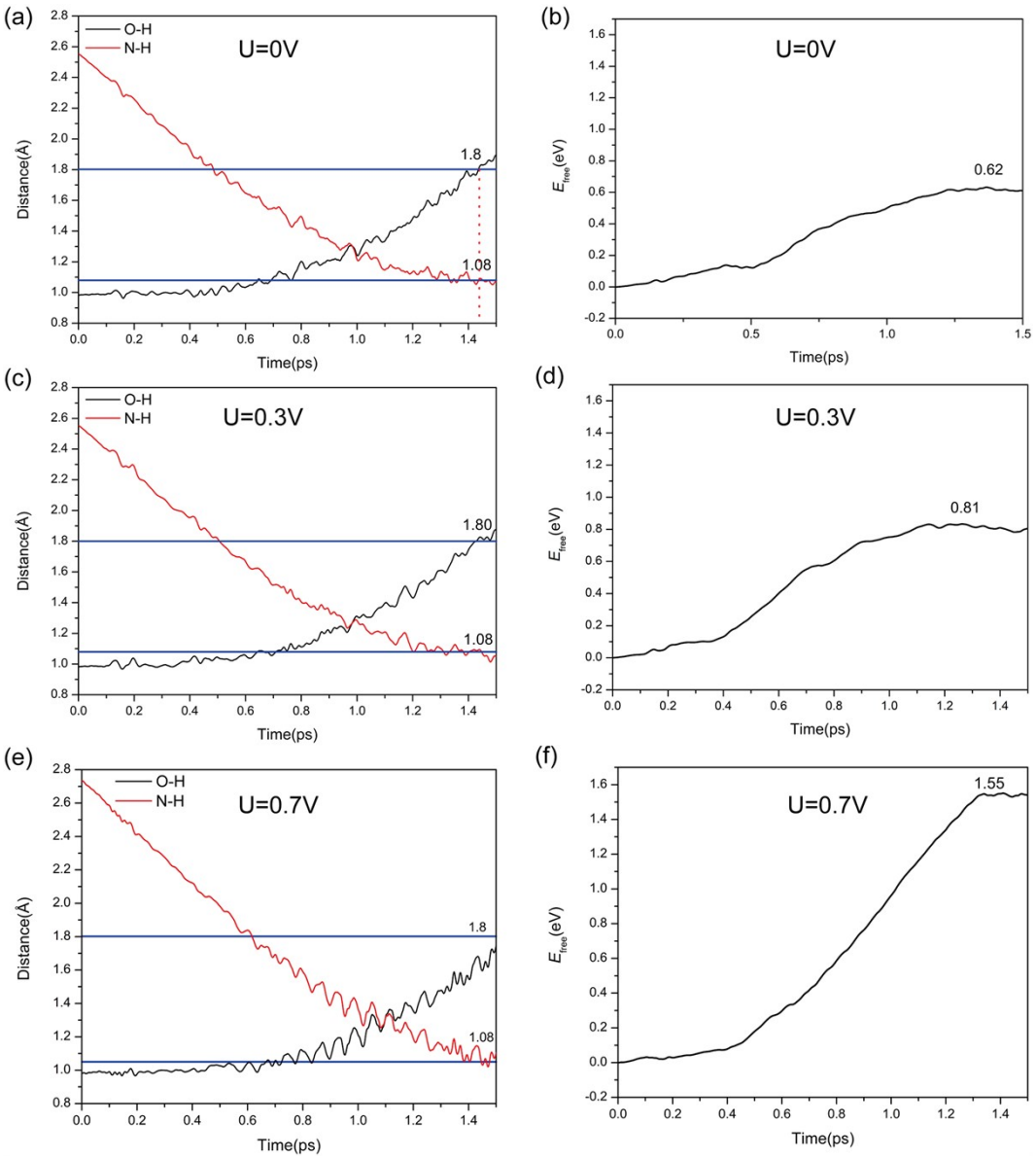

Figure S9. Dynamic evolution of bond lengths of Fe-H and O-H, as well as free energy profiles along the reaction coordinate in the pyrrolic-type FeN_4-explicit system, considering the nitrogen protonation process under various potentials.

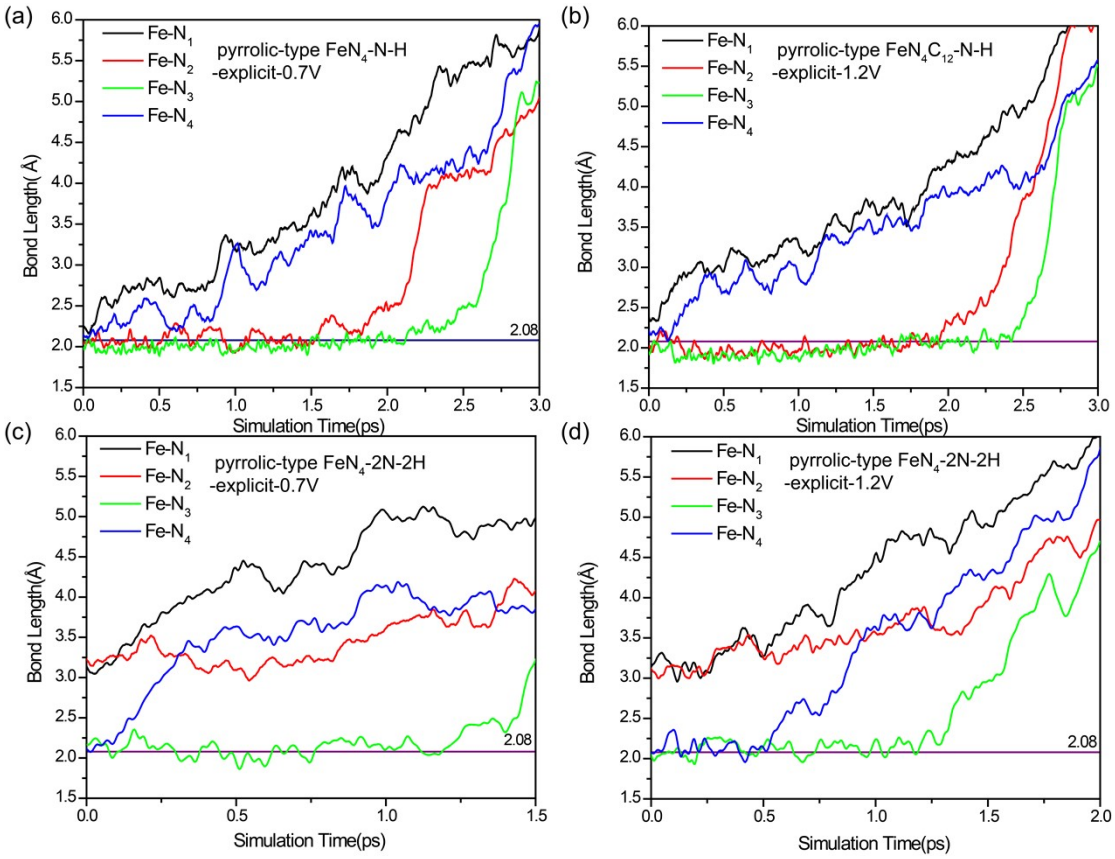

Figure S10. Dynamic evolution of bond lengths of Fe-N(x) along the reaction coordinate in the pyrrolic-type FeN_4-xN-xH-explicit system (x = 1, 2), considering the Fe leaching process under various potentials.

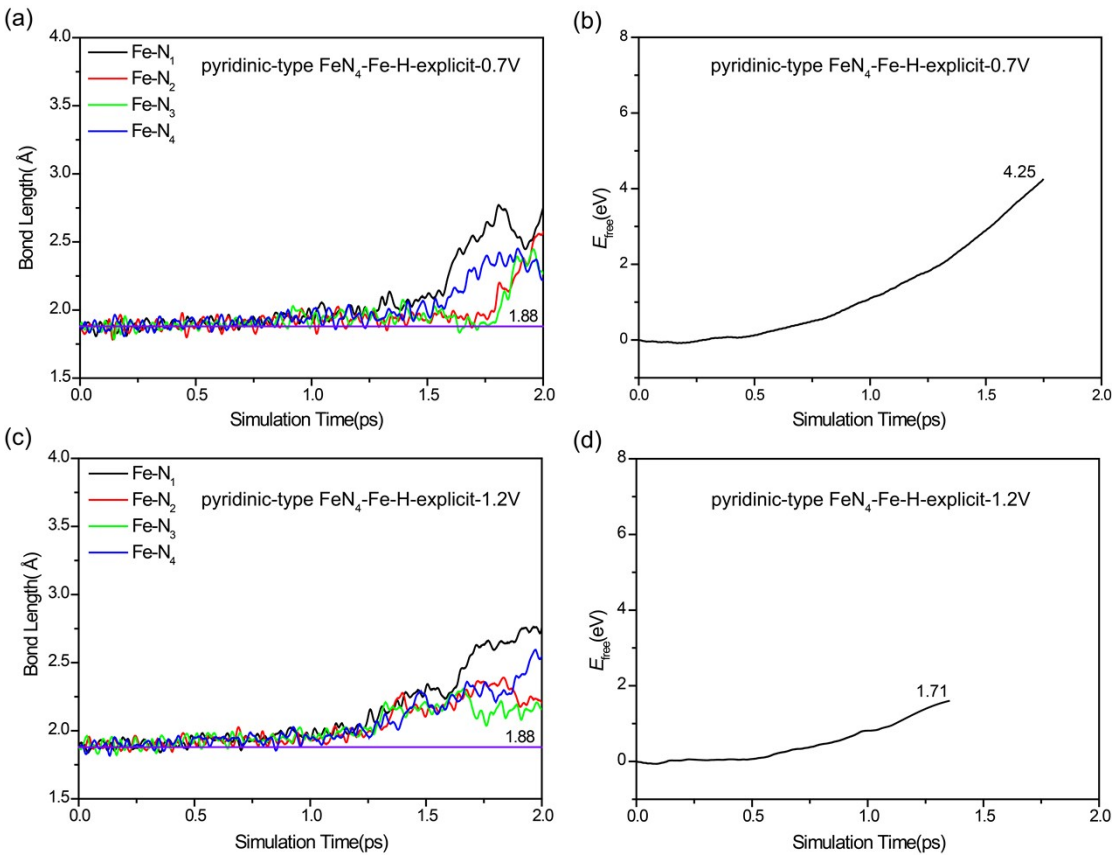

Figure S11. Dynamic evolution of bond lengths of Fe-N(x), as well as free energy profiles along the reaction coordinate in the pyridinic-type FeN_4-Fe-H-explicit system, considering the Fe leaching process under various potentials.

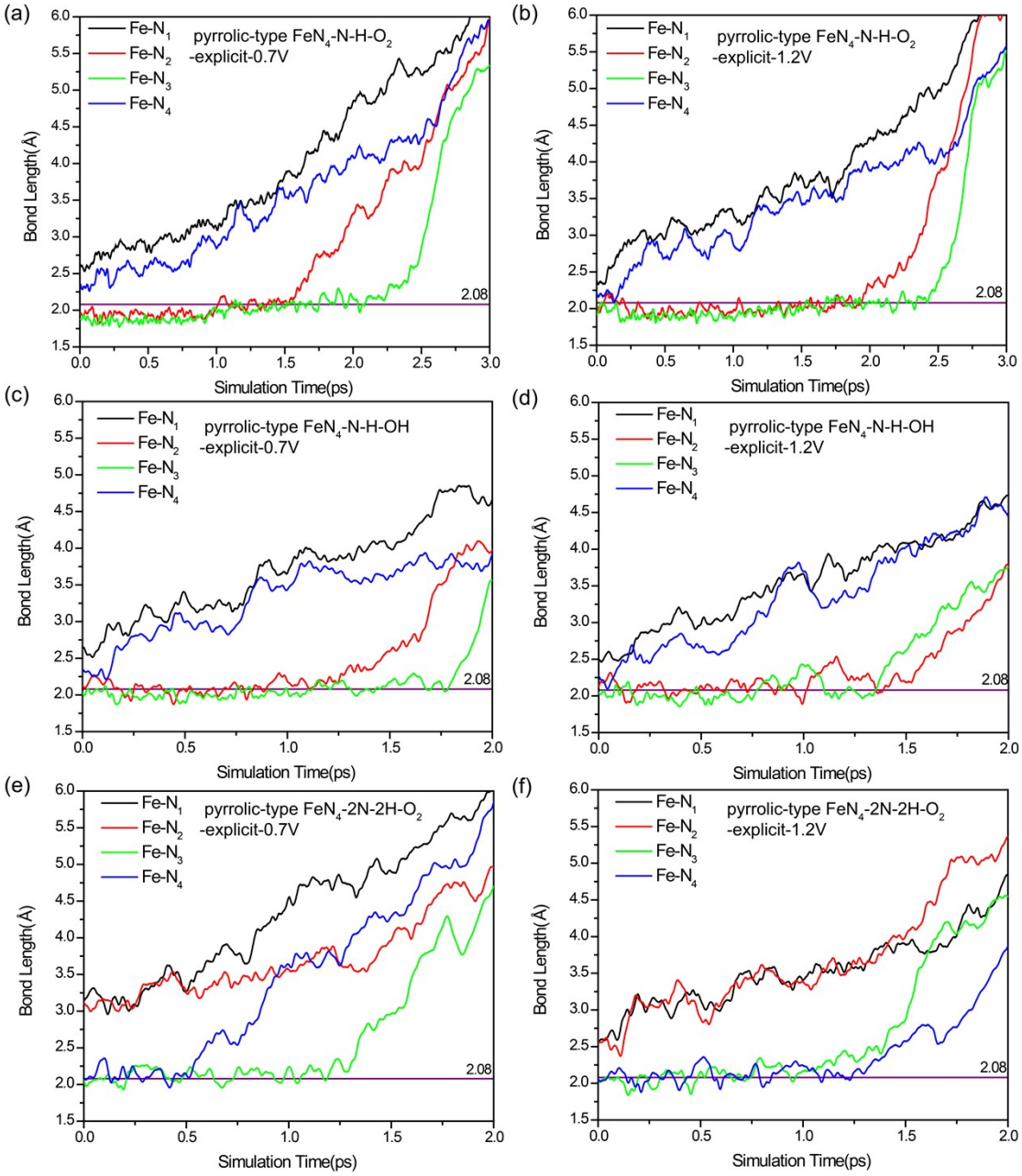

Figure S12. Dynamic evolution of bond lengths of Fe-N(x) along the reaction coordinate in the oxygenated-pyrrolic-type FeN_4-xN-xH-explicit system (x = 1, 2), considering the Fe leaching process under various potentials.

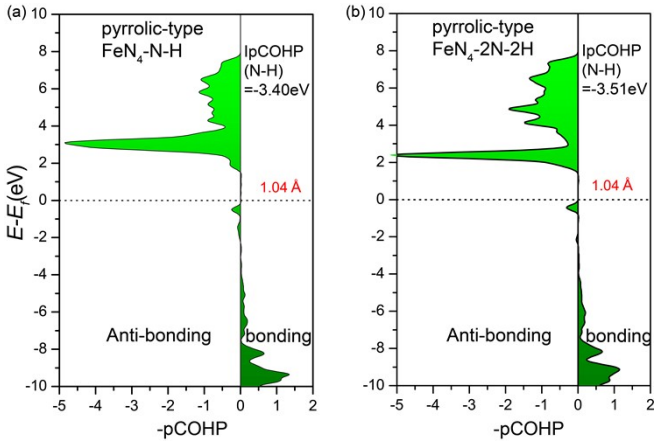

Figure S13. Projected crystal orbital Hamilton population (pCOHP) between the nitrogen atom and hydrogen atom in pyrrolic-type FeN_4 system: (a) 1H and (b) 2H adsorption at N atoms.

References

(1) Chan, K.; Nørskov, J. K., Electrochemical barriers made simple. *J. Phys. Chem. Lett.* **2015**, *6*, 2663-2668.

(2) Chan, K.; Nørskov, J. K., Potential dependence of electrochemical barriers from ab initio calculations. *J. Phys. Chem. Lett.* **2016**, *7*, 1686-1690.

(3) Cheng, T.; Xiao, H.; Goddard III, W. A., Reaction mechanisms for the electrochemical reduction of CO_2 to CO and formate on the Cu (100) surface at 298 K from quantum mechanics free energy calculations with explicit water. *J. Am. Chem. Soc.* **2016**, *138*, 13802-13805.

(4) Mao, K.; Yang, L.; Wang, X.; Wu, Q.; Hu, Z., Identifying iron–nitrogen/carbon active structures for oxygen reduction reaction under the effect of electrode potential. *J. Phys. Chem. Lett.* **2020**, *11*, 2896-2901.

(5) Xie, K.; Wang, F.; Wei, F.; Zhao, J.; Lin, S., Revealing the origin of nitrogen electroreduction activity of molybdenum disulfide supported iron atoms. *J. Phys. Chem. C* **2022**, *126*, 5180-5188.